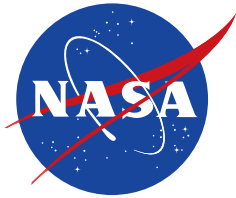


NASA/TP-2005-212862



Stress Analysis of B-52B and B-52H Air-Launching Systems Failure-Critical Structural Components

*William L. Ko
NASA Dryden Flight Research Center
Edwards, California*



April 2005

The NASA STI Program Office...in Profile

Since its founding, NASA has been dedicated to the advancement of aeronautics and space science. The NASA Scientific and Technical Information (STI) Program Office plays a key part in helping NASA maintain this important role.

The NASA STI Program Office is operated by Langley Research Center, the lead center for NASA's scientific and technical information. The NASA STI Program Office provides access to the NASA STI Database, the largest collection of aeronautical and space science STI in the world. The Program Office is also NASA's institutional mechanism for disseminating the results of its research and development activities. These results are published by NASA in the NASA STI Report Series, which includes the following report types:

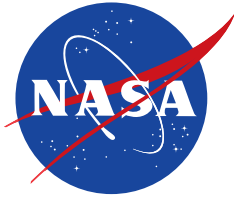
- **TECHNICAL PUBLICATION.** Reports of completed research or a major significant phase of research that present the results of NASA programs and include extensive data or theoretical analysis. Includes compilations of significant scientific and technical data and information deemed to be of continuing reference value. NASA's counterpart of peer-reviewed formal professional papers but has less stringent limitations on manuscript length and extent of graphic presentations.
- **TECHNICAL MEMORANDUM.** Scientific and technical findings that are preliminary or of specialized interest, e.g., quick release reports, working papers, and bibliographies that contain minimal annotation. Does not contain extensive analysis.
- **CONTRACTOR REPORT.** Scientific and technical findings by NASA-sponsored contractors and grantees.
- **CONFERENCE PUBLICATION.** Collected papers from scientific and technical conferences, symposia, seminars, or other meetings sponsored or cosponsored by NASA.
- **SPECIAL PUBLICATION.** Scientific, technical, or historical information from NASA programs, projects, and missions, often concerned with subjects having substantial public interest.
- **TECHNICAL TRANSLATION.** English-language translations of foreign scientific and technical material pertinent to NASA's mission.

Specialized services that complement the STI Program Office's diverse offerings include creating custom thesauri, building customized databases, organizing and publishing research results...even providing videos.

For more information about the NASA STI Program Office, see the following:

- Access the NASA STI Program Home Page at <http://www.sti.nasa.gov>
- E-mail your question via the Internet to help@sti.nasa.gov
- Fax your question to the NASA STI Help Desk at (301) 621-0134
- Telephone the NASA STI Help Desk at (301) 621-0390
- Write to:
NASA STI Help Desk
NASA Center for AeroSpace Information
7121 Standard Drive
Hanover, MD 21076-1320

NASA/TP-2005-212862



Stress Analysis of B-52B and B-52H Air-Launching Systems Failure-Critical Structural Components

*William L. Ko
NASA Dryden Flight Research Center
Edwards, California*

National Aeronautics and
Space Administration

Dryden Flight Research Center
Edwards, California 93523-0273

April 2005

NOTICE

Use of trade names or names of manufacturers in this document does not constitute an official endorsement of such products or manufacturers, either expressed or implied, by the National Aeronautics and Space Administration.

Available from the following:

NASA Center for AeroSpace Information
7121 Standard Drive
Hanover, MD 21076-1320
301-621-0390

National Technical Information Service
5285 Port Royal Road
Springfield, VA 22161
703-605-6000

CONTENTS

	<u>Page</u>
ABSTRACT	1
NOMENCLATURE	1
INTRODUCTION	2
AIR-LAUNCHING SYSTEMS	3
FAILURE-CRITICAL STRUCTURAL COMPONENTS	3
Pegasus [®] Pylon Parts	4
1. Pegasus [®] Pylon Adapter Shackle	4
2. Pegasus [®] Pylon Hook	4
B-52H Pylon Parts	4
1. B-52H Pylon Hook	4
2. B-52H Pylon Front Fitting	4
3. B-52H Pylon Rear Fitting	4
4. B-52H Lower Sway Brace	4
DESCRIPTION OF PROBLEM	5
FINITE-ELEMENT ANALYSIS	5
Finite-Element Modeling	5
Applied Loads	6
Constraints	7
RESULTS	7
Deformations and Stresses	8
1. Pegasus [®] Pylon Adapter Shackle Upper Part	8
2. Pegasus [®] Pylon Adapter Shackle Lower Part	8
3. Pegasus [®] Pylon Hook	9
4. B-52H Pylon Hook	9
5. B-52H Pylon Front Fitting	10
6. B-52H Pylon Rear Fitting	10
7. B-52H Pylon Lower Sway Brace	10
Stress-Load Equations	11
Ultimate, Yield, and Proof Loads	12
CONCLUDING REMARKS	13
FIGURES	14
APPENDIX: MATERIAL PROPERTIES	33
REFERENCES	34

ABSTRACT

The operational life analysis of any airborne failure-critical structural component requires the stress-load equation, which relates the applied load to the maximum tangential tensile stress at the critical stress point. The failure-critical structural components identified are the B-52B-Pegasus^{®*} pylon adapter shackles, B-52B-Pegasus[®] pylon hooks, B-52H airplane pylon hooks, B-52H airplane front fittings, B-52H airplane rear pylon fitting, and the B-52H airplane pylon lower sway brace. Finite-element stress analysis was performed on the said structural components, and the critical stress point was located and the stress-load equation was established for each failure-critical structural component. The ultimate load, yield load, and proof load needed for operational life analysis were established for each failure-critical structural component.

NOMENCLATURE

ALTV	approach and landing test vehicle
B-52B	the NASA “B” model B-52 air launching aircraft
B-52H	the NASA “H” model B-52 air launching aircraft
C	coefficient of Walker crack growth equation, $\frac{\text{in}}{\text{cycle}} \left(\text{ksi} \sqrt{\text{in}} \right)^{-m}$
E	Young’s modulus, lb/in ²
E23	bar element with axial stiffness only
E33	triangular combined membrane and bending element
E43	quadrilateral combined membrane and bending element
G	shear modulus, lb/in ²
JLOC	joint location
K_{IC}	mode I critical stress intensity factor, ksi $\sqrt{\text{in}}$
K_{\max}	mode I stress intensity factor associated with maximum stress of one cycle, ksi $\sqrt{\text{in}}$
m	Walker exponent associated with K_{\max}
n	Walker exponent associated with R
R	stress ratio of one stress cycle $\left(= \frac{\text{minimum stress}}{\text{maximum stress}} \right)$
SRB/DTV	solid rocket booster/drop-test vehicle
t	thickness, in.
V	applied load, lb
V^*	proof load, lb
V_U	ultimate load which causes critical stress point to fail, lb
V_Y	yield load which causes critical stress point to yield, lb
x, y, z	Cartesian coordinates
δ_x	displacement in x direction
δ_y	displacement in y direction
δ_r	displacement in radial direction
η	stress-load coefficient, ksi/lb

*Pegasus[®] is a registered trademark of Orbital Sciences Corporation, Fairfax, Virginia.

θ	angular coordinate measured from x axis, deg
θ_c	angular location of critical stress point measured from x axis, deg
ν	Poisson ratio
σ^*	$= \eta V^*$, tangential tensile stress at critical stress point induced by proof load V^* , ksi
σ_U	ultimate tensile stress, ksi
σ_Y	yield stress, ksi
σ_t	tangential stress along hook inner boundary, ksi
$(\sigma_t)_{\max}$	maximum value of σ_t , ksi
σ_θ	tangential stress in θ direction, ksi
$(\sigma_\theta)_{\max}$	maximum value of σ_θ at critical stress point, ksi
τ_{xy}	shear stress, ksi
$(\tau_{xy})_{\max}$	maximum value of τ_{xy} , ksi
τ_U	ultimate shear stress, ksi

INTRODUCTION

Load-carrying structural components of L-shaped geometry or containing holes usually have stress concentration problems. When subjected to cyclic loading, the peak stress concentration sites can become fatigue-crack initiation sites. Structural components having stress concentration sites may be called failure-critical structural components.

The NASA Dryden (Edwards, California) "B" model B-52 air launch carrier airplane (B-52B) has been used to carry various types of flight research vehicles for high-altitude air-launching tests. The flight-test vehicle is usually mated to the pylon of the B-52B by one L-shaped front hook and two identical L-shaped rear hooks. The L-shaped hook geometry will always induce stress concentration problems in the hook. The critical stress point at the inner curved boundary of the hook, where the tangential tensile stress reaches maximum, is the potential fatigue-crack initiation site (refs. 1–5).

In 1983, during the early flight-test stages of the 49,000-lb solid rocket booster/drop-test vehicle (SRB/DTV), the two old rear hooks (fabricated from 4340 steel) failed almost simultaneously during the towing of the B-52B while it was carrying the SRB/DTV on a relatively smooth taxiway (low-amplitude dynamic loading). It was found that each failed hook had an existing surface microcrack at the critical stress point (ref. 1). The microcracks escaped detection during the preflight inspection because of surface masking by the plating film. These fatigue cracks may have been initiated by a combination of the previous lengthy period of flight-test load cycling and surface corrosion. If the hooks had failed during the takeoff run or during the captive flight, a catastrophic accident might have occurred. This accident underscored the need for reliable and accurate predictions of the operational life of the hooks and other failure-critical structural components of air-launching systems.

The safety of flight tests using the B-52B to carry a drop-test vehicle hinges upon the structural integrity of failure-critical structural components such as the B-52B pylon hooks. It is, therefore, of vital importance to determine the limit of the safe operational lifespan of failure-critical structural components.

Currently the B-52B is being used to carry the 40,000-lb Pegasus[®] rocket-X-43 system through the use of a special adapter, the Pegasus[®] pylon. The thermostructural behavior of the unconventional X-43 (Hyper-X) wing structures was extensively analyzed (ref. 6).

Also, the newly-acquired NASA “H” model B-52 air launching aircraft (B-52H) is to be used to carry the 7,000-lb X-37 approach and landing test vehicle (ALTV). Currently the operational lifespans of the failure-critical components of the Pegasus[®] pylon and B-52H pylon are not known and need to be estimated for safe operational flights.

Before applying the Ko aging theories (ref. 7) to perform the safe operational life analysis of the failure-critical structural components of the B-52B–Pegasus[®] pylon and the B-52H pylon, the stress-load equation, which relates the applied load to the maximum tangential tensile stress induced at the critical stress point, must first be established for each failure-critical structural component.

The purpose of the present report is to document finite-element stress analysis performed to locate the critical stress points and to establish the stress-load equations and the proof loads for the B-52B–Pegasus[®] pylon and B-52H pylon failure-critical structural components.

AIR-LAUNCHING SYSTEMS

In the past, a flight-test vehicle (such as the SRB/DTV or the X-15) could be carried directly by the B-52B pylon hooks because the test vehicle body could nest closely under the concave belly of the pylon as shown in the inset in figure 1. However, for the B-52B pylon to carry the winged Pegasus[®] rocket with the X-43 mated to the Pegasus[®] nose for air launching, as shown in figure 1, a special adapter called the Pegasus[®] pylon is needed. This is because the Pegasus[®] booster rocket has a delta wing, which prevents the Pegasus[®] cylindrical rocket body from nesting closely under the concave belly of the B-52B pylon. The Pegasus[®] pylon is to be carried by the B-52B pylon hooks through a double-shear pin that will hang from the B-52B front hook, and by Pegasus[®] pylon adapter shackles that will connect to the two rear hooks of the B-52B pylon, figure 2. The Pegasus[®] rocket–X-43 system is then carried by four identical Pegasus[®] pylon hooks, shown in figure 3.

The double-shear pin is not failure-critical because there is no stress concentration problem. The two Pegasus[®] pylon adapter shackles are highly failure-critical, however, because each shackle has a rectangular hole (fig. 2) with four sharp rounded corners in the upper part and a circular pinhole at the lower part—the sites of stress concentrations. Also, the Pegasus[®] pylon hooks are L-shaped and thus are definitely failure-critical.

Figure 4 shows the newly-acquired B-52H carrying the X-37 ALTV using two identical L-shaped pylon hooks. The pylon is attached to the wing of the B-52H by two identical front fittings and one rear fitting (fig. 4). Figures 5(a)–(d), respectively, show the failure-critical structural components of the B-52H pylon, which are identified as the B-52H pylon hooks [fig. 5(a)], the B-52H pylon front fitting [fig. 5(b)], the B-52H pylon rear fitting [fig. 5(c)], and the B-52H pylon lower sway brace [fig. 5(d)].

FAILURE-CRITICAL STRUCTURAL COMPONENTS

In this section, the failure-critical structural components of the B-52B–Pegasus[®] adapter pylon and the B-52H pylon are briefly described.

Pegasus[®] Pylon Parts

1. Pegasus[®] Pylon Adapter Shackle

The geometry of a typical Pegasus[®] shackle is shown in figure 2. The Pegasus[®] pylon shackles are made of PH13-8Mo stainless steel. The two 0.812-inch-thick Pegasus[®] shackles are failure-critical because each upper part has a rectangular hole (1.438 by 1.514 in.) with four rounded corners with a small radius of curvature of 0.093 in. (the inner boundary of the B-52B rear hook has a 0.5-inch radius of curvature). The shackle lower part contains a circular pin-loaded hole of 1.25-inch diameter. Thus, the Pegasus[®] adapter shackle upper and lower parts have stress concentration problems and are, therefore, failure-critical.

2. Pegasus[®] Pylon Hook

The Pegasus[®] pylon has four identical L-shaped hooks (fig. 3) made of AMAX MP 35N alloy (the same material used for the two rear hooks of the B-52B pylon). The geometry of a typical Pegasus[®] pylon hook is shown in figure 3. This hook has thickness of $t = 2$ in., and an 0.51-inch inner radius. The outer curved boundary has a 3.48-inch radius of curvature centered at a different location (fig. 3).

B-52H Pylon Parts

1. B-52H Pylon Hook

Figure 4 shows the B-52H carrying the X-37 ALTV using two identical L-shaped hooks, which are made of PH13-8Mo stainless steel. The dimensions of a typical B-52H pylon hook are shown in figure 5(a). The B-52H pylon hook, very similar to the B-52B special pylon hooks carrying the X-38 drop-test vehicle (ref. 9), has a thickness of $t = 2.8$ in., and a 0.5-inch inner boundary radius of curvature (identical to that of the B-52B rear pylon hook which thickness is $t = 1.1$ in.).

2. B-52H Pylon Front Fitting

Figure 5(b) shows the geometry of the B-52H pylon typical front fitting, which is fabricated from PH13-8Mo stainless steel. The upper vertical triangular flange is 1.125 in. thick, with a circular hole of 1.379 in. radius, and an outer arc boundary of 2.390 in. radius. The triangular region has a base angle of approximately 42.63 deg.

3. B-52H Pylon Rear Fitting

Figure 5(c) shows the geometry of the B-52H pylon rear fitting, which is fabricated from PH13-8Mo stainless steel. The rear fitting has two identical lugs, each of which has a thickness of $t = 0.39$ in. and a circular hole of 1.495 in. diameter, with a curved boundary of 1.55 in. radius. The remaining key dimensions are indicated in figure 5(c).

4. B-52H Lower Sway Brace

Figure 5(d) shows the geometry of B-52H pylon lower sway brace, which is fabricated from PH13-8Mo stainless steel. The lower sway brace has four identical lugs, each of which has a thickness of $t = 0.50$ in., a circular

hole of 1.00 in. diameter, and a curved outer boundary of 1.00 in. radius. The remaining key dimensions are indicated in figure 5(d).

DESCRIPTION OF PROBLEM

Before the safe operational life analysis can be performed for the failure-critical structural components, the following stress-load equation

$$(\sigma_t)_{\max} = \eta V \quad (1)$$

associated with the critical stress point must first be established for each failure-critical structural component. In equation (1), V is the applied load, and $(\sigma_t)_{\max}$ [= $(\sigma_\theta)_{\max}$ for a circular boundary] is the maximum tangential tensile stress induced at the critical stress point, which is related to V through the stress-load coefficient η .

The purpose of the problem is to perform finite-element stress analysis to study the stress field, to locate the critical stress point (θ_c), to determine the value of η of equation (1), and to establish the proof load V^* for each failure-critical structural component.

FINITE-ELEMENT ANALYSIS

For the finite-element stress analysis of the failure-critical structural components, the Structural Performance And Resizing (SPAR) computer program (ref. 8) was used in the linear-elasticity stress analysis.

Finite-Element Modeling

Figures 6–12 show, respectively, the finite-element models generated for the Pegasus[®] pylon adapter shackle upper part, the Pegasus[®] pylon adapter shackle lower part, the Pegasus[®] pylon hook, the B-52H new pylon hook, the B-52H pylon front fitting, the B-52H pylon rear fitting, and the B-52H pylon lower sway brace. For the Pegasus[®] pylon adapter shackle upper part, only the upper right region was modeled because of the symmetric nature (fig. 6). Only the right-hand side region of the Pegasus[®] pylon adapter shackle lower part (fig. 7) was modeled due to symmetry with respect to the vertical centerline (y axis). For the Pegasus[®] pylon hook and the B-52H new pylon hook, only the stress-critical lower regions were modeled. Only one-half of the upper vertical triangular region of the B-52H pylon front fitting was modeled due to symmetry with respect to the vertical axis (y axis, fig. 10). For the B-52H pylon rear fitting, only one lug region was modeled (fig. 11). As well, only one lug region of the B-52H pylon lower sway brace was modeled (fig. 12).

The quadrilateral plate elements (E43 elements) and triangular plate elements (E33 elements) were used in all of the finite-element modeling.

The Pegasus[®] pylon shackle lower part, B-52H pylon front fitting, B-52H pylon rear fitting, and B-52H pylon lower sway brace are circular-pin loaded. Therefore, bar elements (E23 elements with axial stiffness only) were used to model the lubricated loading pins. The E23 elements were used to maintain the shapes of the elastic loading pins, and to simulate the lubricated loading-pin surfaces because they introduce no shear resistance. For each inclusion, the E23 elements are divided into two groups. The first group is for modeling one half-disk on the loading side and the second set is used to model the half-disk on the slacking side. The two centers of the half-pin models were intentionally made noncoincident and were not connected elastically. Thus, the loading on one

group will not be transmitted to the other group, thereby simulating the loose interfacial contact between the loading pin and the unloaded hole boundary. The sizes of the finite-element models are shown in table 1.

Table 1. Sizes of finite-element models.

Critical structural components	Number			
	JLOC	E23 elements	E33 elements	E43 elements
Pegasus [®] pylon shackle upper	3938	----	274	3662
Pegasus [®] pylon shackle lower	1859	41	24	1717
Pegasus [®] pylon hook	1277	----	38	1160
B-52H pylon hook	1243	----	48	1152
B-52H pylon front fitting	1087	21	34	995
B-52H pylon rear fitting	1731	81	37	1620
B-52H pylon lower sway brace	1091	45	33	978

Note: The input material properties of the above structural components are listed in the appendix.

Applied Loads

The applied loads V on the different critical structural components are listed in table 2.

Table 2. Applied loads V used on different critical structural components.

Structural component	V , lb
Pegasus [®] pylon shackle upper	57,819*
Pegasus [®] pylon shackle lower	57,819*
Pegasus [®] pylon hook	57,819*
B-52H pylon hook	57,819*
B-52H pylon front fitting	245,563 [†]
B-52H pylon rear fitting	33,224.5 [†]
B52H pylon lower sway brace	26,983.75 [†]

* Proof load for the B-52B pylon rear hooks.

[†] Stress analysis estimated ultimate load of 245,563 lb contains 68,000 lb preload.

It must be mentioned that the applied loads shown in table 2 are for establishing the stress-load relationship for each structural component, and that for the linear elasticity stress analysis, the magnitudes of the applied loads are inconsequential.

For the loading on the Pegasus[®] adapter shackle, Pegasus[®] hook, and B-52H pylon hook, identical loads (table 2) were applied. This vertical load is the previously-used proof load for the B-52B pylon rear hooks ($V^* = 57,819$ lb). The reason for using the same loads for those three components is to compare the levels of peak tangential tensile stresses at the respective critical stress points of the three components subjected to the same load.

For the Pegasus[®] pylon adapter shackle upper part model, because of symmetry, only one-half of the upward load ($V/2 = 28,909.5$ lb) was uniformly distributed over the nodes lying within a 0.55-inch region (in contact with half the thickness of the B-52B pylon rear hook) on the inner horizontal surface of the Pegasus[®] pylon adapter shackle upper part model (fig. 6). For each critical part containing a circular hole (figs. 7, 10, 11, and 12) the pin load on the hole boundary was converted to nodal forces over the upper boundary of the hole with sine distribution. For the Pegasus[®] pylon hook (fig. 8) and the B-52H new pylon hook (fig. 9), the downward hook loads were distributed over the respective upper horizontal boundaries of the hooks.

For the B-52H lower sway brace, the outward pin load is applied in the $\theta = -13$ deg direction (fig. 12).

Constraints

For the Pegasus[®] pylon adapter shackle upper part and lower part models (figs. 6 and 7) the horizontal cutoff boundary is constrained to have free motion only in the x direction, and the vertical cutoff boundary only in the y direction. Both of the cutoff boundaries have zero rotation about the z axis to simulate material continuity. The lubricated boundary guides are represented with rollers (figs. 6 and 7). For the Pegasus[®] pylon adapter shackle lower part model (fig. 6), the upper left corner node is fixed and is indicated with a double triangular symbol.

For the Pegasus[®] pylon hook and the B-52H new pylon hook models (figs. 8 and 9), the upper inner corner node of each model is fixed in space (indicated with a triangular symbol), and the upper boundaries are allowed to move along the guides as indicated with rollers.

For the B-52H pylon front and rear fitting models (figs. 10 and 11), the lower left corner node of each model is fixed (indicated with a double triangular symbol), and the horizontal and vertical boundaries are allowed to have free motions only in one direction along the lubricated guides and are represented with trains of rollers (figs. 10 and 11).

For the B-52H pylon lower sway brace, the vertical edge of the model is fixed (fig. 12), and the outward applied load is in the $\theta = -13$ deg direction. The methods of modeling the pin loading are the same as the approaches described earlier.

RESULTS

The deformations and stress distributions obtained from the finite-element stress analysis of the failure-critical structural components are presented in the following sections.

Deformations and Stresses

1. Pegasus® Pylon Adapter Shackle Upper Part

Figure 13 shows the deformed shape of the Pegasus® pylon adapter shackle upper part. Note that the horizontal region bent upward with a maximum upward displacement of $\delta_y = 0.895 \times 10^{-2}$ in. along the vertical axis of symmetry. The vertical region bent inward with a maximum horizontal inward displacement of $\delta_x = -0.474 \times 10^{-2}$ in.

Figure 14 shows the distribution of tangential stress σ_t along the inner boundary of the Pegasus® pylon adapter shackle upper part. The critical stress point is located on the inner rounded corner boundary at an angle $\theta_c = 15.75^\circ$ measured from the horizontal x axis. The applied hook load $V = 57,819$ lb induced $(\sigma_t)_{\max} = 279.740$ ksi which exceeded the yield stress $\sigma_Y = 190$ ksi, and caused the region $-4^\circ < \theta < 47^\circ$ of the inner boundary to be in the plastic zone; it also exceeded the ultimate tensile stress $\sigma_U = 201$ ksi in the region $-2^\circ < \theta < 43^\circ$. Keep in mind that the present stress analysis is limited to linear elasticity. If elasto-plastic effect is considered, the value of $(\sigma_t)_{\max}$ could be much lower.

Figure 15 shows the distribution of tangential stress σ_t along the depth of the tension-critical cross section ($\theta_c = 15.75^\circ$), and also along the $y = -0.664$ -inch horizontal line of the Pegasus® pylon adapter shackle upper part. Notice that away from the stress-critical point, the depth-wise stress distribution became practically linear. Also, the depth of the induced plastic zone is extremely shallow.

Figure 16 shows the distribution of shear stress τ_{xy} along the depth of the shear-critical cross section of the Pegasus® pylon adapter shackle upper part. The maximum shear stress is located near the inner boundary and is only $(\tau_{xy})_{\max} = 56.992$ ksi, which is about 49 percent of the shear failure stress $\tau_U = 117$ ksi. Based on figures 14 or 15, the stress-load equation for the Pegasus® pylon adapter shackle upper part is established as

$$(\sigma_t)_{\max} = 4.8382 \times 10^{-3} V \quad (2)$$

2. Pegasus® Pylon Adapter Shackle Lower Part

Figure 17 shows the deformed shape of the Pegasus® pylon adapter shackle lower part. The applied load $V = 57,819$ lb induced a downward displacement of $\delta_y = -0.616 \times 10^{-2}$ in. at the pinhole boundary bottom point.

Figure 18 shows the distribution of tangential stress σ_θ along the hole boundary of the Pegasus® pylon adapter shackle lower part. The critical stress point is located on the hole boundary at an angle $\theta_c = -11.25$ deg measured from the horizontal x axis. The applied hook load $V = 57,819$ lb induced the peak tangential tensile stress $(\sigma_\theta)_{\max} = 152.896$ ksi (80 percent of yield stress $\sigma_Y = 190$ ksi of PH13-8Mo) at the critical stress point ($\theta_c = -11.25$ deg, fig. 18). Notice that the pinhole boundary is under considerable compression in the upper region of $50^\circ < \theta < 90^\circ$ and also in the lower region of $-90^\circ < \theta < -56^\circ$.

Figure 19 shows the distribution of tangential stress σ_θ along the depth of the tension-critical cross section ($\theta_c = -11.25^\circ$) of the Pegasus® pylon adapter shackle lower part. The decrease in the value of σ_θ in the depth direction from the critical stress point is not as steep as in that of the Pegasus® pylon adapter shackle upper part (fig. 15). Based on figures 18 or 19, the stress-load equation for the Pegasus® adapter shackle lower part is established as

$$(\sigma_{\theta})_{\max} = 2.6444 \times 10^{-3} V \quad (3)$$

3. Pegasus[®] Pylon Hook

Figure 20 shows the deformed shape of the Pegasus[®] pylon hook. The applied load $V = 57,819$ lb induced the downward vertical displacement of $\delta_y = 0.112 \times 10^{-1}$ in. at the horizontal tip of the hook.

Figure 21 shows the distribution of tangential stress σ_t along the inner boundary of the Pegasus[®] pylon hook. The critical stress point is located on the inner rounded boundary at an angle $\theta_c = -20.76^\circ$ measured from the horizontal x axis (fig. 20). The induced peak tangential tensile stress at the stress-critical point is $(\sigma_t)_{\max} = 141.420$ ksi (60 percent of AMAX yield stress $\sigma_Y = 235$ ksi).

Figure 22 shows the distribution of tangential stress σ_t along the depth of the tension-critical cross section ($\theta_c = -20.76^\circ$) of the Pegasus[®] pylon hook. The tangential stress σ_t turned to slightly negative (compression) near the outer boundary of the hook.

Figure 23 shows the distribution of shear stress τ_{xy} along the depth of the shear-critical cross section of the Pegasus[®] pylon hook. The point of peak shear stress $(\tau_{xy})_{\max} = 24.160$ ksi (17 percent of AMAX shear failure stress $\tau_U = 141$ ksi) is located slightly beneath the load-applied horizontal upper boundary. Notice that the shear stress distribution profile is saddle-shaped, and is quite similar to that in the X-38 hook (ref. 9) because of similar hook geometry. Based on figures 21 or 22, the stress-load equation for the Pegasus[®] pylon hook is established as

$$(\sigma_t)_{\max} = 2.4459 \times 10^{-3} V \quad (4)$$

4. B-52H Pylon Hook

Figure 24 shows the deformed shape of the B-52H new pylon hook. The hook load $V = 57,819$ lb induced the downward vertical displacement of $\delta_y = -0.705 \times 10^{-2}$ in. at the hook horizontal tip.

Figure 25 shows the distribution of tangential stress σ_t along the inner boundary of the B-52H pylon hook. The critical stress point is located on the inner boundary at an angle $\theta_c = -27^\circ$ measured from the horizontal x axis (fig. 25). The peak tangential tensile stress at the critical stress point is $(\sigma_t)_{\max} = 51.370$ ksi (27 percent of PH13-8Mo yield stress $\sigma_Y = 190$ ksi).

Figure 26 shows the distribution of tangential stress σ_t along the depth of the tension-critical cross section ($\theta_c = -27^\circ$) of the B-52H pylon hook. Like the Pegasus[®] pylon hook (fig. 22), the tangential stress σ_t turned to slightly negative (compression) toward the outer boundary of the hook.

Figure 27 shows the distribution of shear stress τ_{xy} along the depth of the shear-critical cross section of the B-52H pylon hook. The peak shear stress $(\tau_{xy})_{\max} = 6.807$ ksi (5.8 percent of PH13-8Mo shear failure stress $\tau_U = 117$ ksi) is at a point slightly beneath the upper horizontal surface. Again, the shear stress distribution profile is saddle-shaped, and is very similar to that of the X-38 hook (ref. 9) because of similar hook geometry. Based on figures 25 or 26, the stress-load equation for the B-52H pylon hook is established as

$$(\sigma_t)_{\max} = 0.9064 \times 10^{-3} V \quad (5)$$

5. B-52H Pylon Front Fitting

Figure 28 shows the deformed shape of the B-52H pylon front fitting. The applied upward load $V = 245,563$ lb induced the upward vertical displacement of $\delta_y = 0.179 \times 10^{-1}$ in. at the pinhole upper boundary. Figure 29 shows the distribution of tangential stress σ_θ along the inner boundary of the pinhole. The critical stress point of the stress concentration is located on the inner boundary at angular location $\theta_c = 6.75^\circ$ measured from the horizontal x axis. The induced peak tangential tensile stress at the critical stress point is $(\sigma_\theta)_{\max} = 202.209$ ksi (and slightly exceeded the PH13-8Mo tensile failure stress $\sigma_U = 201$ ksi). This applied load is practically an ultimate load. The boundary tangential stress σ_θ exceeded PH13-8Mo yield stress $\sigma_Y = 190$ ksi in the region $0 < \theta < 20^\circ$.

Figure 30 shows the distribution of tangential stress σ_θ along the tension-critical stress line ($\theta_c = 6.75^\circ$) of the B-52H pylon front fitting. Based on figures 29 or 30, the stress-load equation for the B-52H pylon front fitting is established as

$$(\sigma_\theta)_{\max} = 0.8235 \times 10^{-3} V \quad (6)$$

6. B-52H Pylon Rear Fitting

Figure 31 shows the deformed shape of the B-52H pylon rear fitting. The applied upward load $V = 33,224.5$ lb induced the upward vertical displacement of $\delta_y = 0.746 \times 10^{-2}$ in. at the pinhole top boundary. Figure 32 depicts the distribution of tangential stress σ_θ along the inner boundary of the pinhole. Notice that there are two stress concentration points. The first point is located on the inner boundary at $\theta = 2.25^\circ$ with tangential stress $\sigma_\theta = 102.338$ ksi (54 percent of PH13-8Mo tensile strength $\sigma_Y = 190$ ksi). The second point, which is the critical stress point, is located on the inner boundary at an angle $\theta_c = 173.25^\circ$ measured from the x axis, with peak tangential tensile stress $(\sigma_\theta)_{\max} = 106.640$ ksi (56 percent of PH13-8Mo tensile strength $\sigma_Y = 190$ ksi). Figure 33 shows the distribution of tangential stress σ_θ along the $\theta = 2.25^\circ$ radial line, and also along the $\theta_c = 173.25^\circ$ critical stress line. Based on figures 32 or 33, the stress-load equation for the B-52H pylon rear fitting is established as

$$(\sigma_\theta)_{\max} = 3.2097 \times 10^{-3} V \quad (7)$$

7. B-52H Pylon Lower Sway Brace

Figure 34 shows the deformed shape of the B-52H pylon lower sway brace. The applied pin load $V = 26,983.75$ lb induced the outward displacement $\delta_r = 0.308 \times 10^{-2}$ in. at the pinhole outer boundary and along the loading direction ($\theta = -13^\circ$). Figure 35 shows the distribution of tangential stress σ_θ along the inner boundary of the pinhole. Notice that there are two stress concentration points. The first point is located on the inner boundary at $\theta = 74.25^\circ$ with tangential stress $\sigma_\theta = 141.572$ ksi (75 percent of PH13-8Mo yield stress $\sigma_Y = 190$ ksi). The second point, which is the critical stress point, is located on the inner boundary at an angle $\theta_c = -101.25^\circ$ measured from the x axis with the peak tangential tensile stress $(\sigma_\theta)_{\max} = 143.476$ ksi (76 percent of PH13-8Mo yield stress $\sigma_Y = 190$ ksi). Figure 36 shows the distribution of tangential stress σ_θ along the $\theta = 74.25^\circ$ radial line, and also along the $\theta_c = -101.25^\circ$ critical stress line. Based on figures 35 or 36, the stress-load equation for the B-52H pylon lower sway brace is established as

$$(\sigma_\theta)_{\max} = 5.3164 \times 10^{-3} V \quad (8)$$

Stress-Load Equations

Through the finite-element stress analysis, the critical stress point was located, and the associated stress-load coefficient η was established for the stress-load equation (1) for each failure-critical structural component [eqs. (2)–(8)]. Table 3 summarizes the stress-load coefficients η and the angular locations θ_c of the critical stress points for all the analyzed failure-critical structural components. In table 3, the previous B-52B hook data (refs. 1 and 2) are also included for comparison.

Table 3. Finite-element established stress-load coefficients (η) and angular locations (θ_c) of the critical stress points of the analyzed failure-critical structural components.

Structural component	η , ksi/lb	θ_c , deg
B-52B front hook*	7.3522×10^{-3}	-26.25
B-52B left rear hook*	5.8442×10^{-3}	-27.75
B-52B right rear hook*	5.8442×10^{-3}	-27.75
Pegasus® shackles upper	4.8382×10^{-3}	15.75
Pegasus® shackles lower	2.6444×10^{-3}	-11.25
Pegasus® pylon hooks	2.4459×10^{-3}	-20.76
B-52H pylon hook	0.9064×10^{-3}	-27.00
B-52H pylon front fitting	0.8235×10^{-3}	6.75
B-52H pylon rear fitting	3.2097×10^{-3}	173.25
B-52H pylon lower sway brace	5.3164×10^{-3}	-101.25

* Established earlier (refs. 1 and 2).

As shown in table 3, under the same B-52B rear hook loading, the η value (or critical stress level) for the Pegasus® pylon shackle upper part is about 83 percent of that for the B-52B pylon rear hooks, even though the radius of curvature of the rounded corner (0.093 in.) of the Pegasus® pylon shackle upper part is much smaller than that of the B-52B rear hook (0.5 in.). This is because each of the rounded corners (upper or lower) of the Pegasus® pylon shackle upper part is loaded with only one-half of the applied load and, therefore, the critical stress level (or η value) of the Pegasus® pylon shackle turned out to be lower than that of the B-52B rear hook. However, because PH13-8Mo stainless steel was used instead of AMAX alloy, which is the material used for the B-52B rear hooks, the operational lifespan of the Pegasus® pylon shackle upper part may not necessarily be higher, and remains to be analyzed.

Ultimate, Yield, and Proof Loads

Based on the values of η listed in table 3 and equation (1), the ultimate load V_U , which will cause the critical point stress to reach the ultimate stress σ_U , can be calculated from

$$V_U = \frac{\sigma_U}{\eta} \quad (9)$$

and the yield load V_Y , which will cause the critical point stress to reach the yield stress σ_Y , can be calculated from

$$V_Y = \frac{\sigma_Y}{\eta} \quad (10)$$

Finally, the proof load V^* may be calculated from the following proof-load equation

$$V^* = 1.25 \times \left(\frac{V_U}{2.25} \right) = 0.5556 \frac{\sigma_U}{\eta} \quad (11)$$

which defined V^* as 1.25 times the limit load, $V_U/2.25$.

Table 4 lists the ultimate loads, yield loads, and proof loads calculated for different failure-critical structural components.

Table 4. Ultimate loads V_U , yield loads V_Y , and proof loads V^* for failure-critical structural components established by finite-element linear elasticity stress analysis.

Structural component	σ_U , ksi	σ_Y , ksi	V_U , lb	V_Y , lb	V^* , lb	V^*/V_Y
B-52B front hook	175	145	23,802	19,722	13,223(36,500)*	0.67(1.85)*
B-52B rear hooks	250	235	42,777	40,211	23,765(57,819)*	0.59(1.44)*
Pegasus [®] pylon shackle upper	201	190	41,544	39,271	23,080	0.59
Pegasus [®] pylon shackle lower	201	190	76,010	71,850	42,228	0.59
Pegasus [®] pylon hook	250	235	102,212	6,079	56,784(75,000)*	0.59(0.78)*
B-52H pylon hook	201	190	221,756	209,620	123,198	0.59
B-52H pylon front fitting	201	190	244,080	230,723	135,600	0.59
B-52H pylon rear fitting	201	190	62,623	59,196	34,791	0.59
B-52H pylon lower sway brace	201	190	37,808	35,738	21,004	0.59

* Values used in the earlier proof-load tests (refs. 3–5).

In table 4, the proof loads V^* used in the earlier proof-load tests (refs. 3–5) of the B-52B hooks and the Pegasus[®] pylon hooks are shown in parentheses. The earlier proof loads V^* exceeded their respective yield loads V_Y ($V^* > V_Y$), and will certainly induce a plastic zone in the vicinity of the critical stress points. This may be beneficial because, after the release of the proof load, the plastic zone generated will be under compression. This compressive stress field could reduce the operational tensile stresses and thereby improve the fatigue life of the failure-critical structural components. For a ($V^* > V_Y$) case, elasto-plastic stress analysis is required to determine the exact extent of the plastic zone induced around the critical stress point. The analysis of the pre-stress problem is currently underway.

CONCLUDING REMARKS

Finite-element stress analysis was conducted on the failure-critical structural components of the B-52B–Pegasus[®] and B-52H airplane pylons. The results of the analysis are summarized below.

1. The critical stress point was located for each failure-critical structural component.
2. The stress-load equation (to be used for the operational life analysis) was established for each failure-critical structural component.
3. The lower value of stress-load coefficient η implies lower induced tangential tensile stress at the critical stress point.
4. If the three B-52B airplane pylon hooks are included in the comparison with the other failure-critical structural components, the B-52B airplane pylon front hook has the highest value of η , and the B-52H airplane pylon front fitting has the lowest value of η .
5. The proof load was established for each failure-critical structural component for future operational life analysis.
6. All of the proof loads used earlier for the B-52B airplane pylon hooks exceeded their respective yield loads.
7. The proof load exceeding the yield load ($V^* > V_Y$) may be beneficial because, after the release of the proof load, the induced plastic zone will be under a compressive pre-stress field, which could reduce the operational tensile stresses and thereby improve the operational life of the failure-critical structural components.

*Dryden Flight Research Center
National Aeronautics and Space Administration
Edwards, California, June 20, 2004*

FIGURES

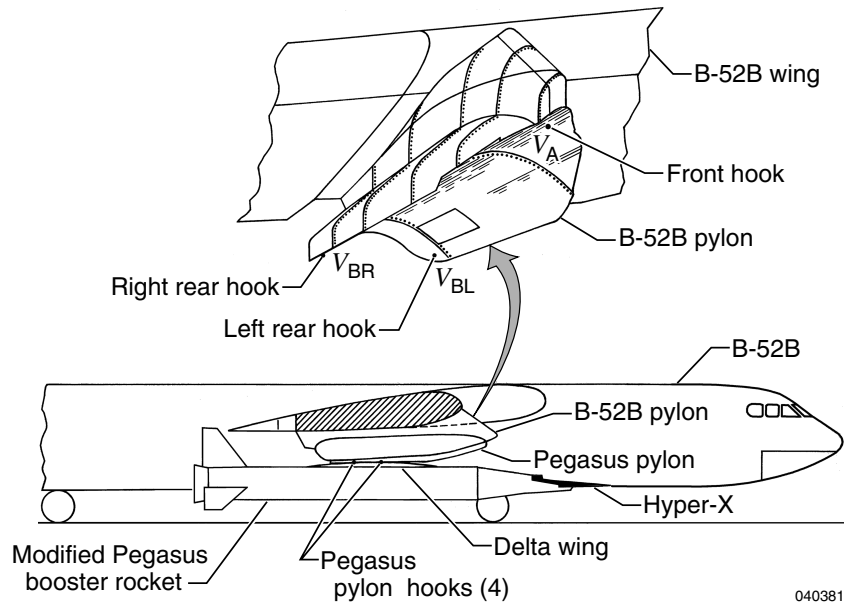


Figure 1. The B-52B carrying different types of air-launching flight-test vehicles.

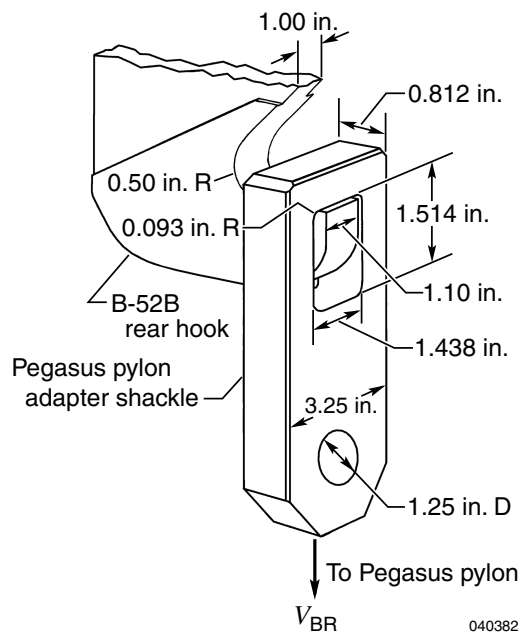


Figure 2. Geometry of the Pegasus[®] pylon adapter shackle connected to the B-52B pylon rear hook; dimensions in inches.

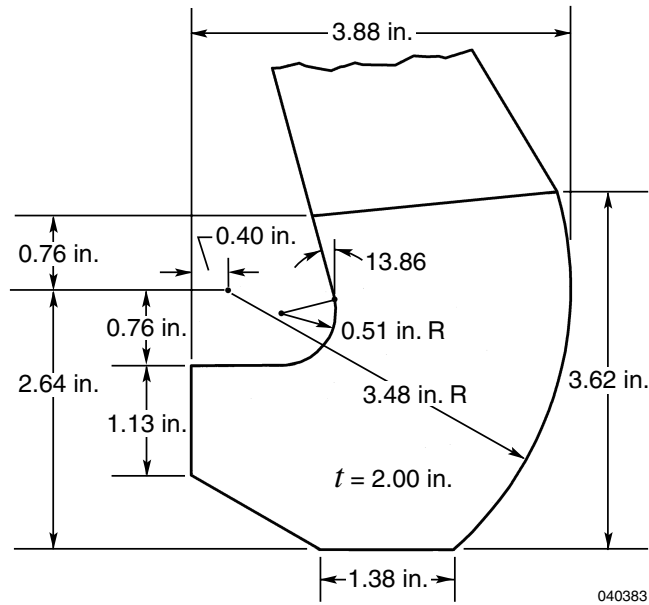


Figure 3. Geometry of the Pegasus[®] pylon hook; dimensions in inches.

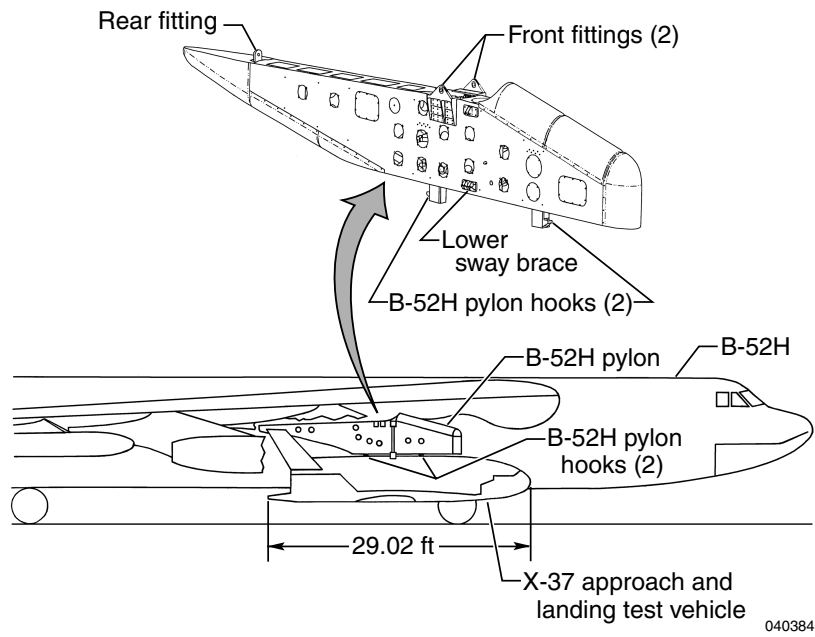
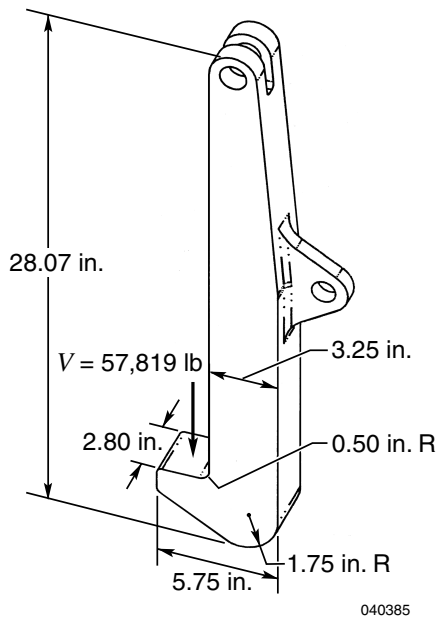
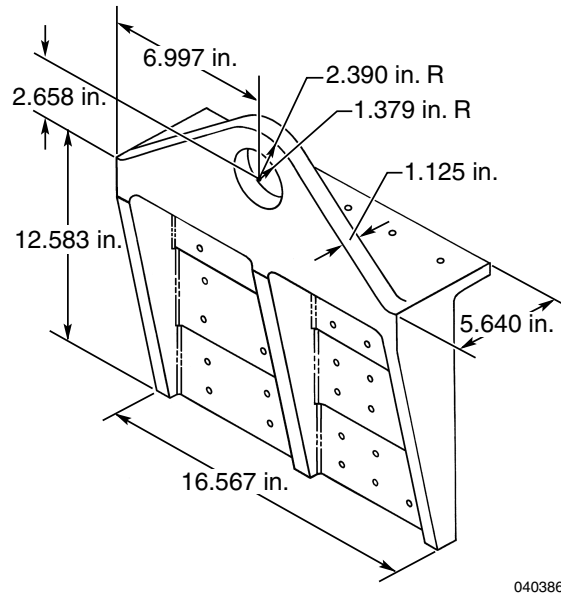


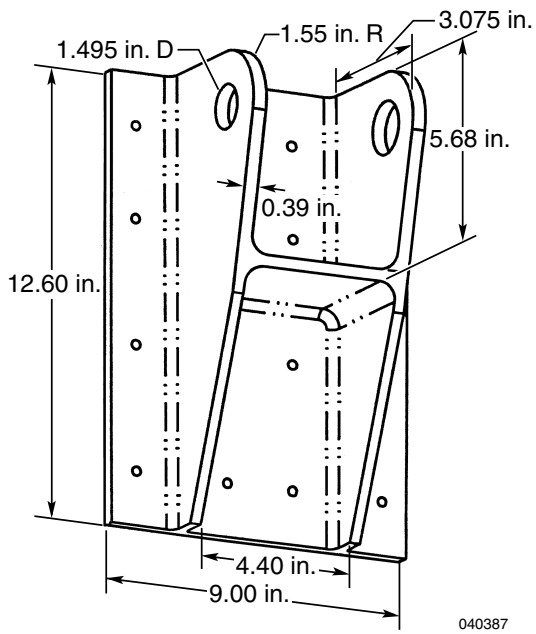
Figure 4. The B-52H carrying the X-37 approach and landing test vehicle (ALTV).



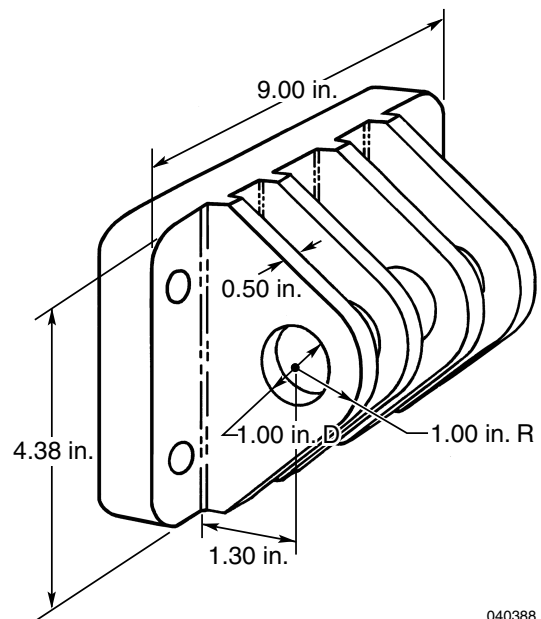
(a) B-52H pylon hook.



(b) B-52H pylon front fitting.



(c) B-52H pylon rear fitting.



(d) B-52H pylon lower sway brace.

Figure 5. Geometry of the B-52H airplane new pylon hook; dimensions in inches.

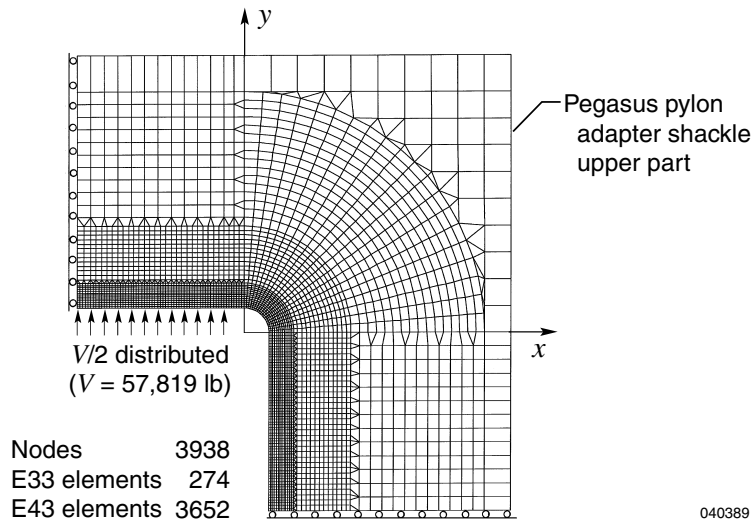


Figure 6. Finite-element model for the Pegasus[®] pylon adapter shackle upper part.

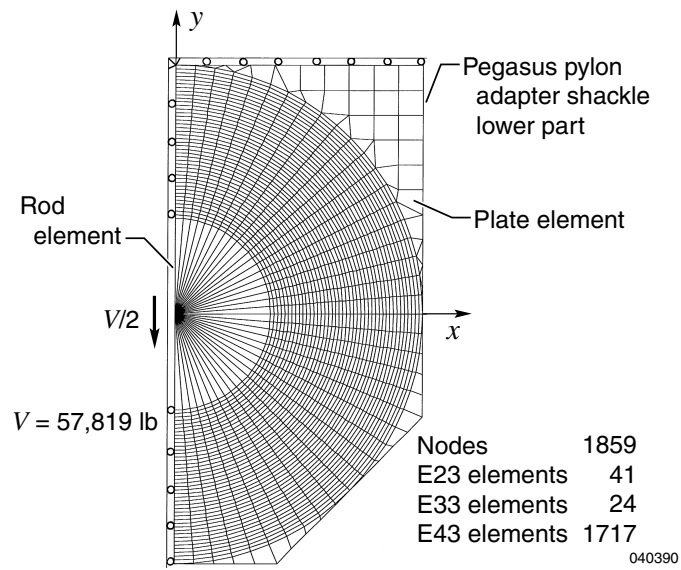


Figure 7. Finite-element model for the Pegasus[®] pylon adapter shackle lower part.

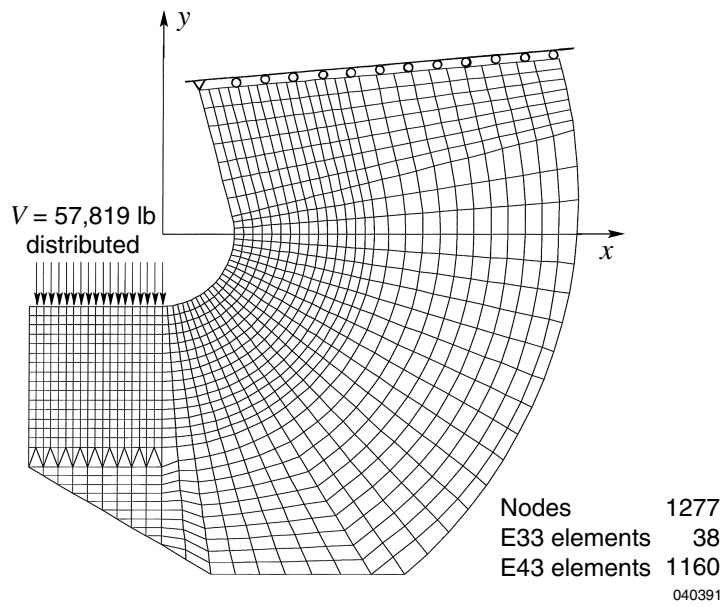


Figure 8. Finite-element model for the Pegasus[®] pylon hook.

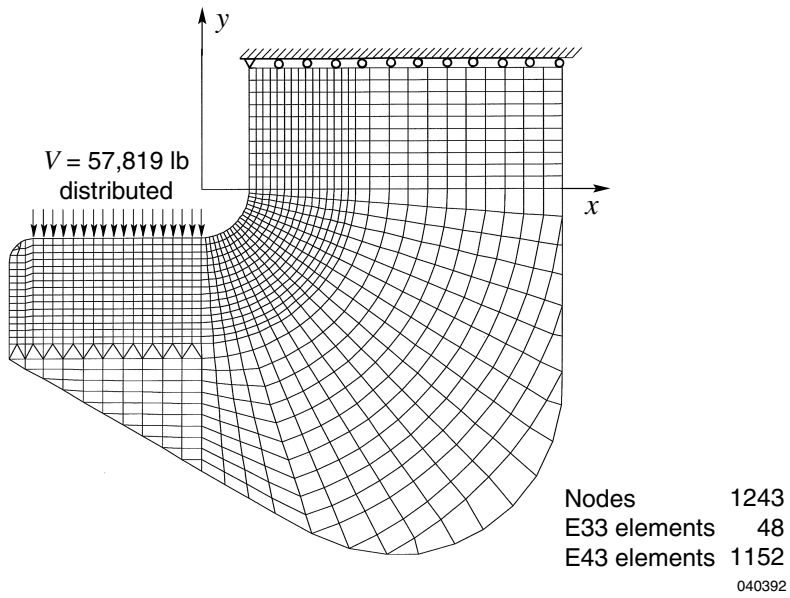


Figure 9. Finite-element model for the B-52H new pylon hook.

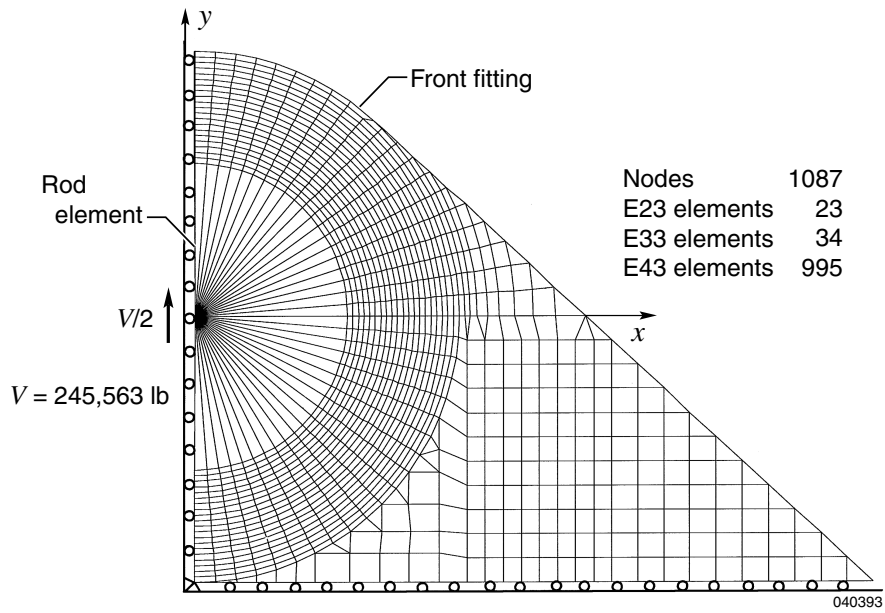


Figure 10. Finite-element model generated for the B-52H pylon front fitting.

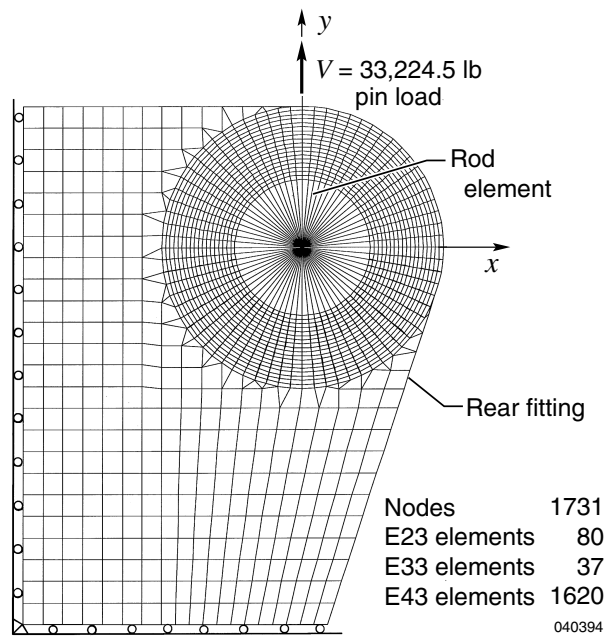


Figure 11. Finite-element model generated for the B-52H pylon rear fitting.

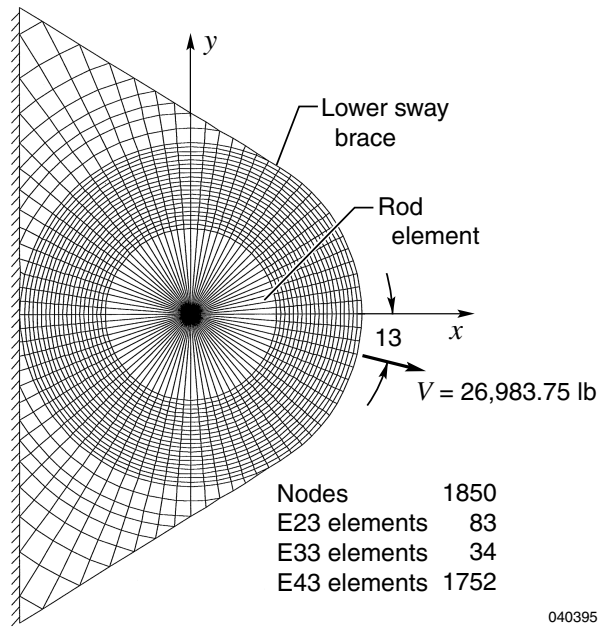


Figure 12. Finite-element model generated for the B-52H pylon lower sway brace.

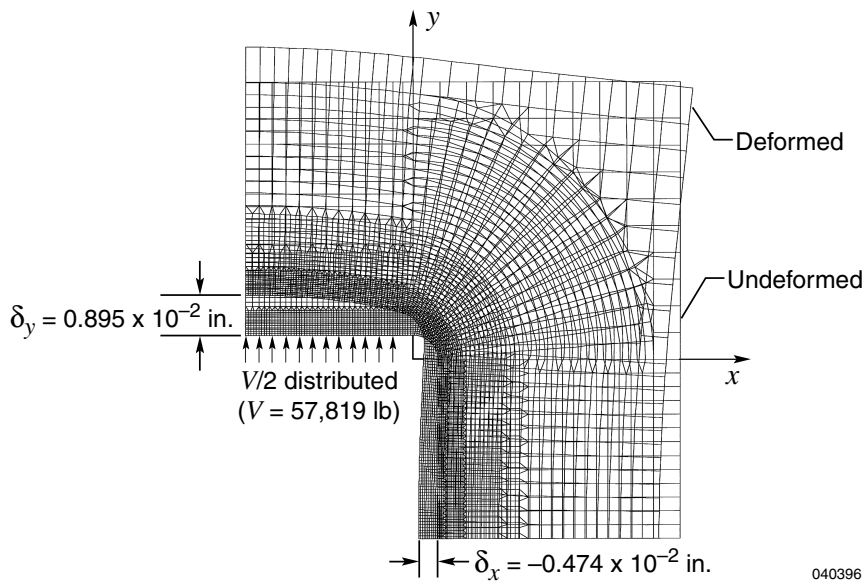
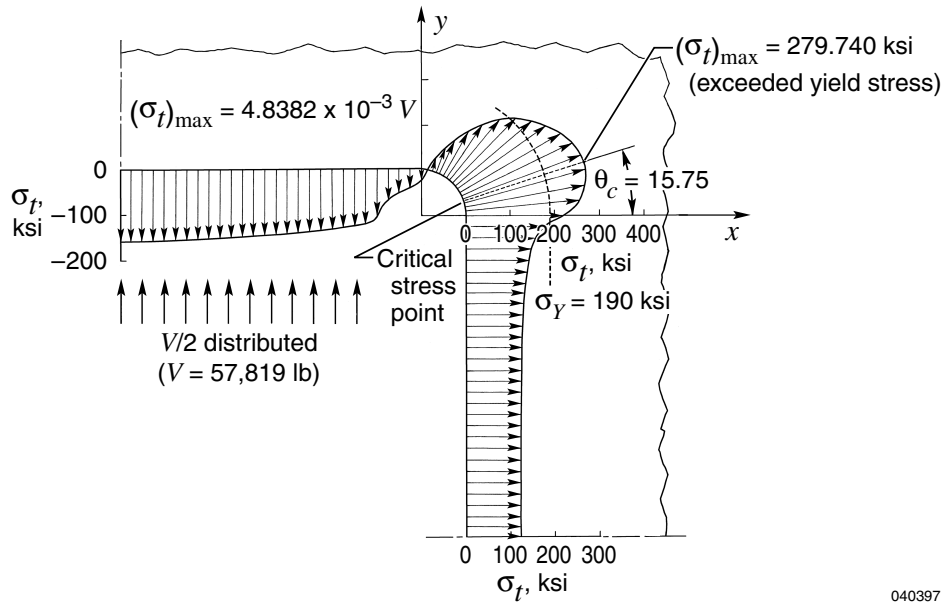
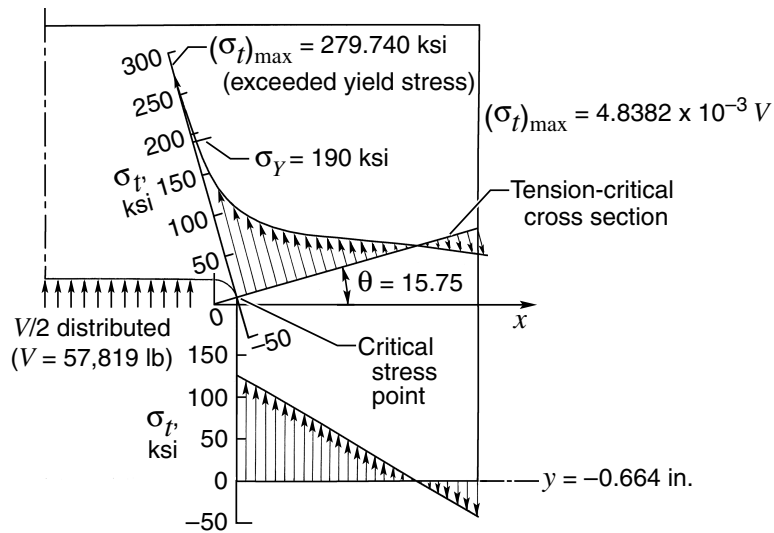


Figure 13. Deformed shape of the Pegasus[®] pylon adapter shackle upper part.



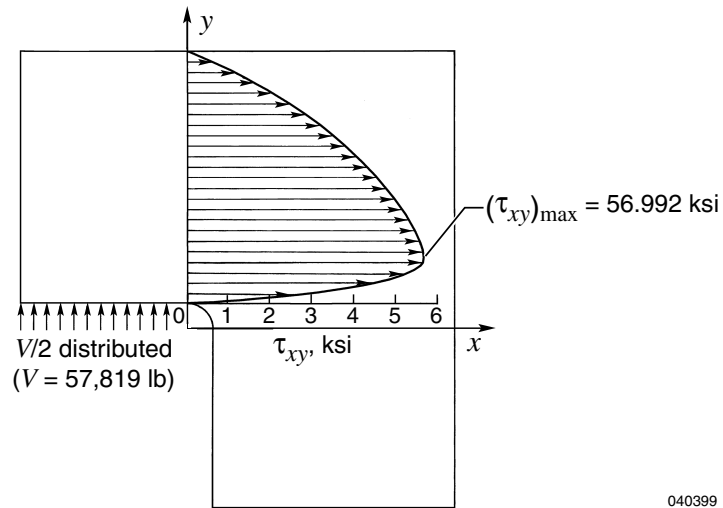
040397

Figure 14. Distribution of tangential stress σ_t along the inner boundary of the Pegasus[®] pylon adapter shackle upper part.



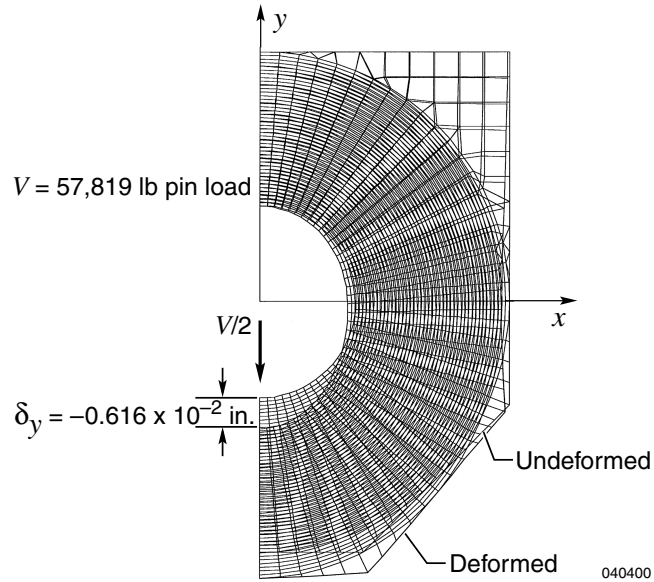
040398

Figure 15. Distribution of tangential stress σ_t along $\theta_c = -15.75^\circ$ line and along $y = -0.664$ in. line of the Pegasus[®] pylon adapter shackle upper part.



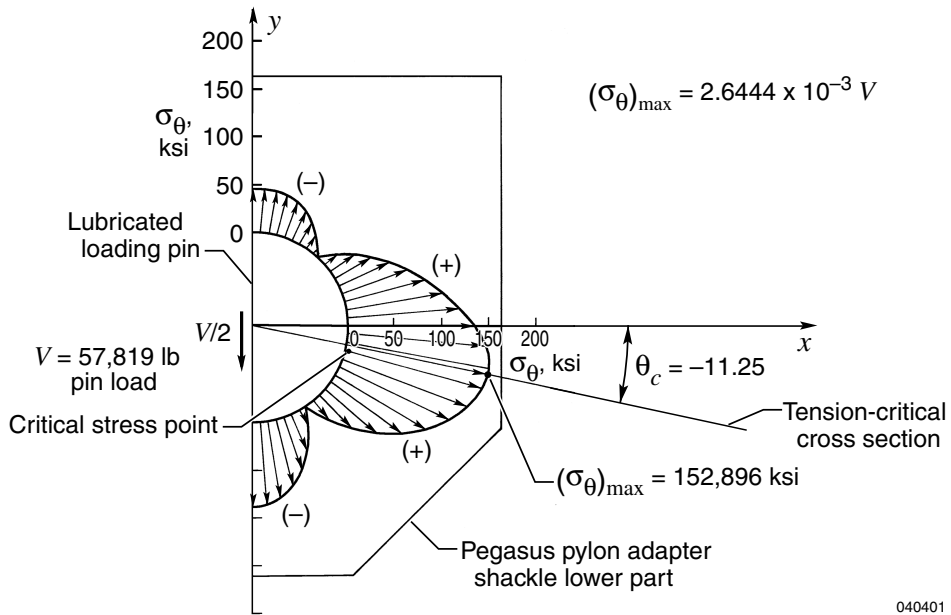
040399

Figure 16. Distribution of shear stress τ_{xy} along the depth of the Pegasus® pylon adapter shackle upper part shear-critical cross section.



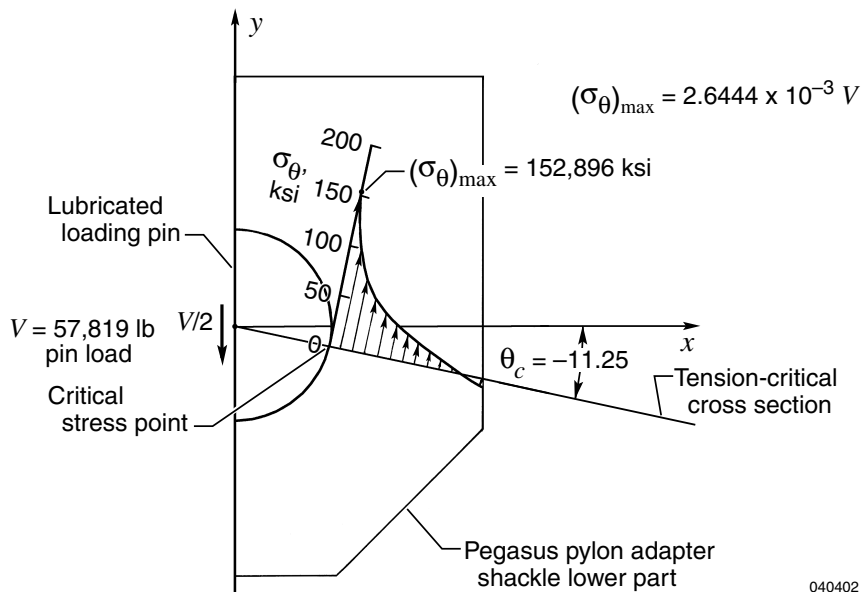
040400

Figure 17. Deformed shape of the Pegasus® pylon adapter shackle lower part.



040401

Figure 18. Distribution of tangential stress σ_θ along the hole boundary of the Pegasus[®] pylon adapter shackle lower part.



040402

Figure 19. Distribution of tangential stresses σ_θ along the depth of the tension-critical cross section of the Pegasus[®] pylon adapter shackle lower part.

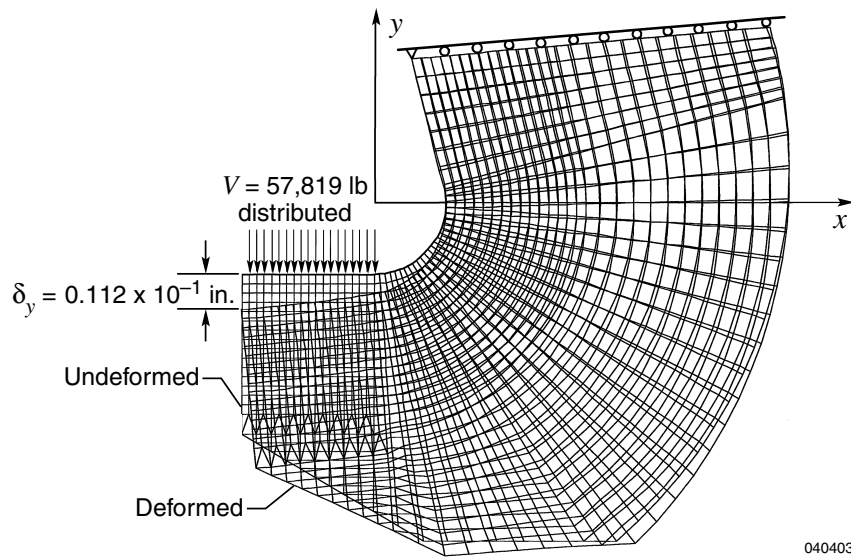


Figure 20. Deformed shape of the Pegasus[®] pylon hook.

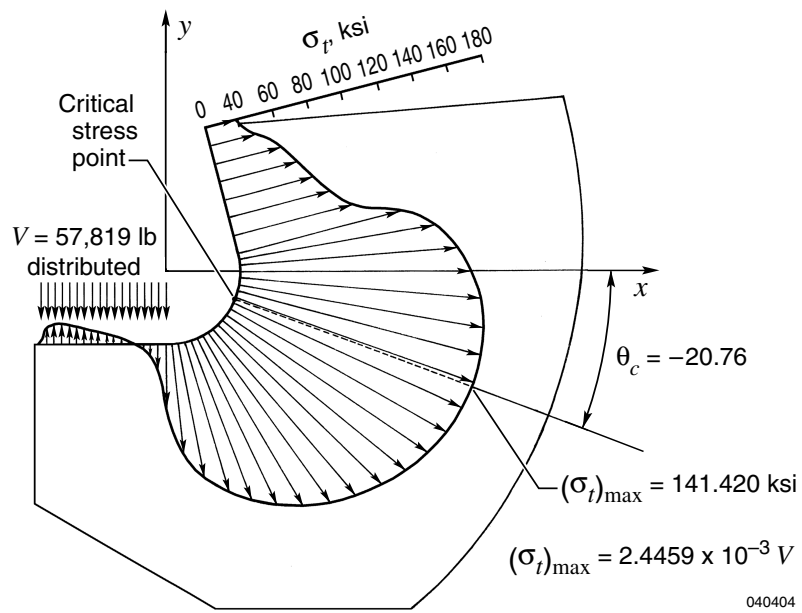


Figure 21. Distribution of tangential stress σ_t along the inner boundary of the Pegasus[®] pylon hook.

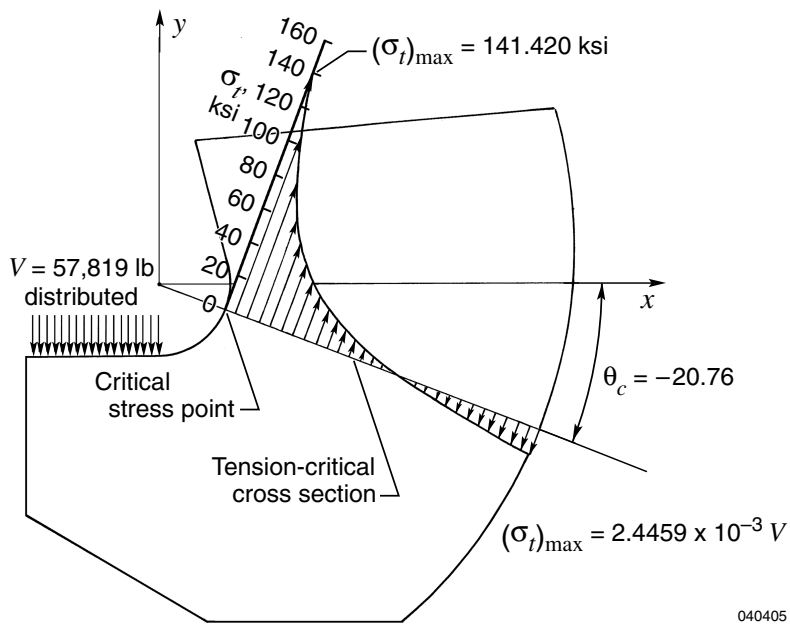


Figure 22. Distribution of tangential stress σ_t along the depth of the tension-critical cross section of the Pegasus[®] pylon hook.

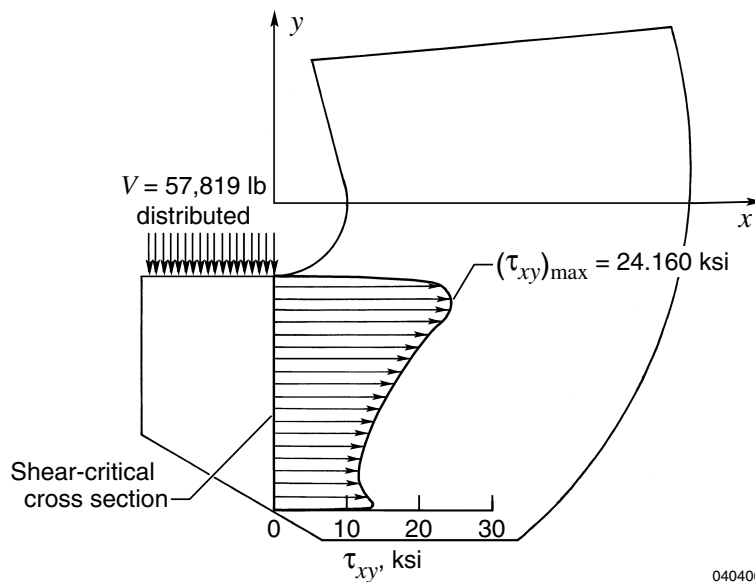


Figure 23. Distribution of shear stress τ_{xy} along the depth of the shear-critical cross section of the Pegasus[®] pylon hook.

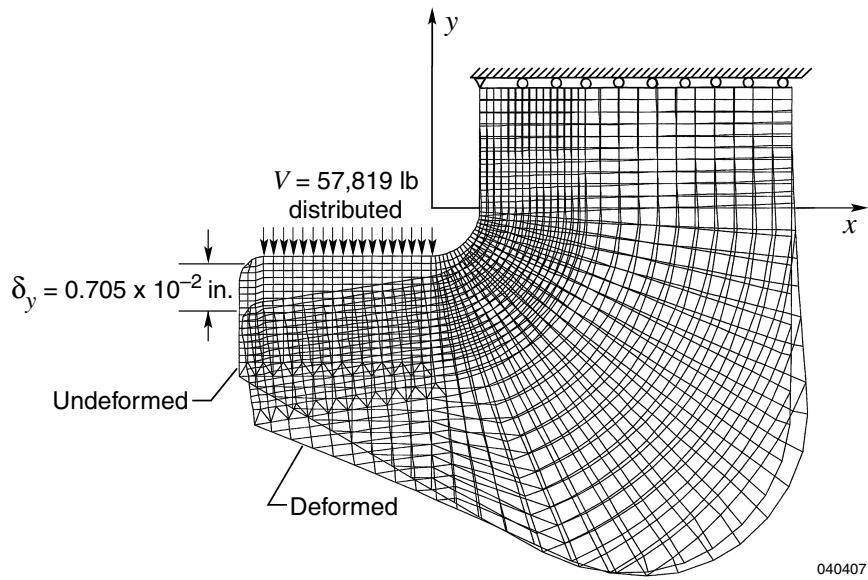


Figure 24. Deformed shape of B-52H new pylon hook.

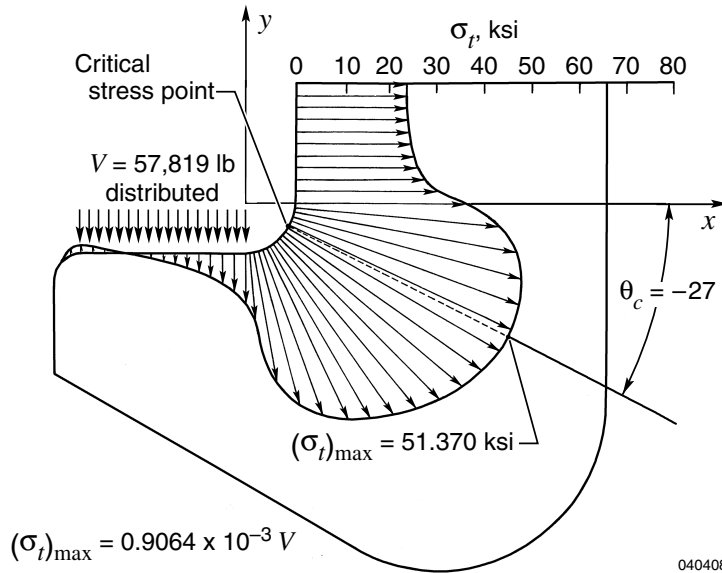


Figure 25. Distribution of tangential stress σ_t along the inner boundary of the B-52H pylon hook.

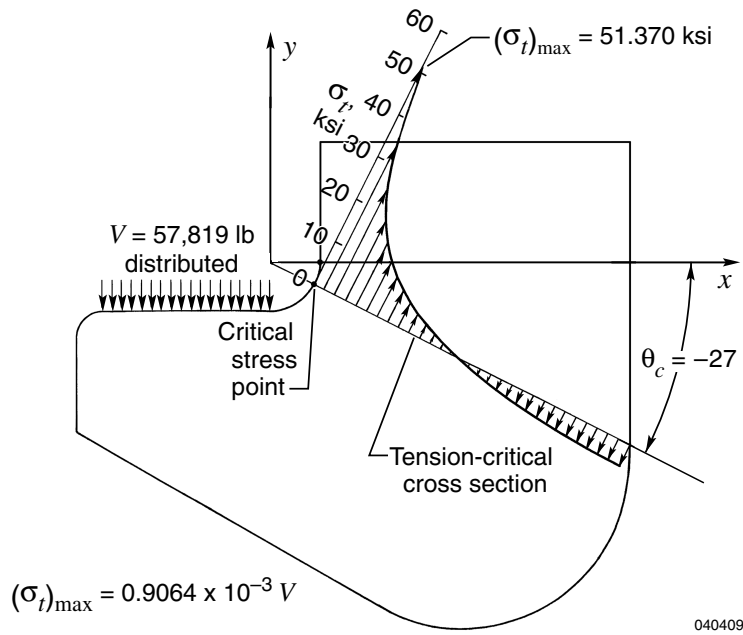


Figure 26. Distribution of tangential stress σ_t along the depth of the tension-critical cross section of the B-52H pylon hook.

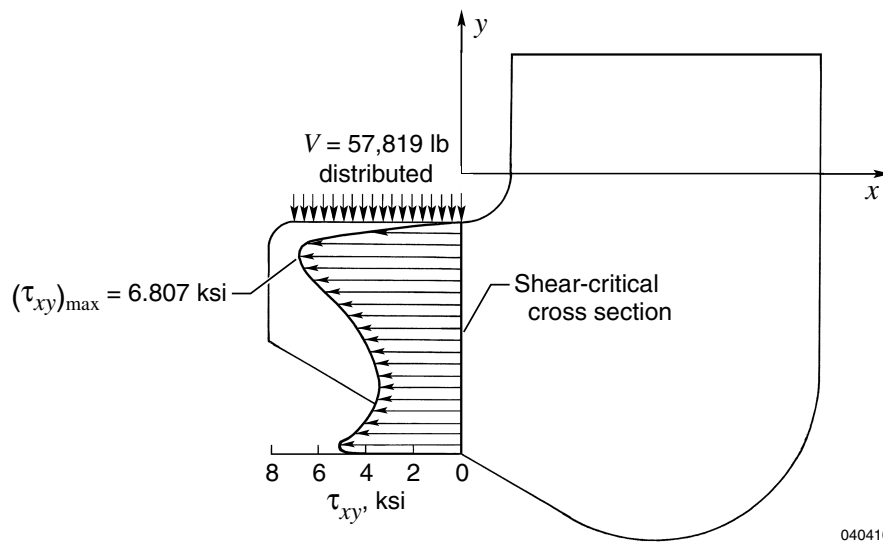


Figure 27. Distribution of shear stress τ_{xy} along the depth of the shear-critical cross section of the B-52H pylon hook.

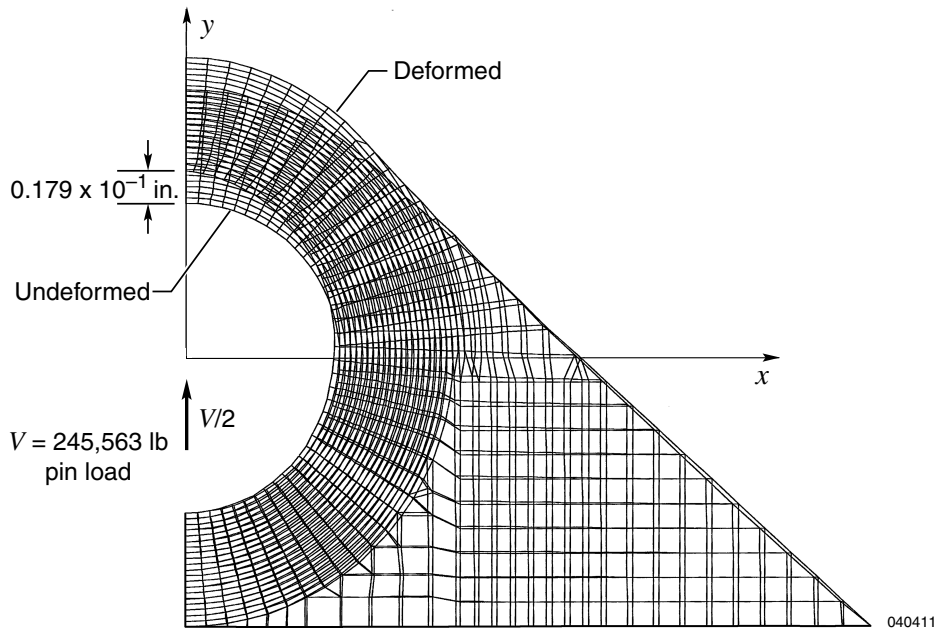


Figure 28. Deformed shape of the B-52H pylon front fitting.

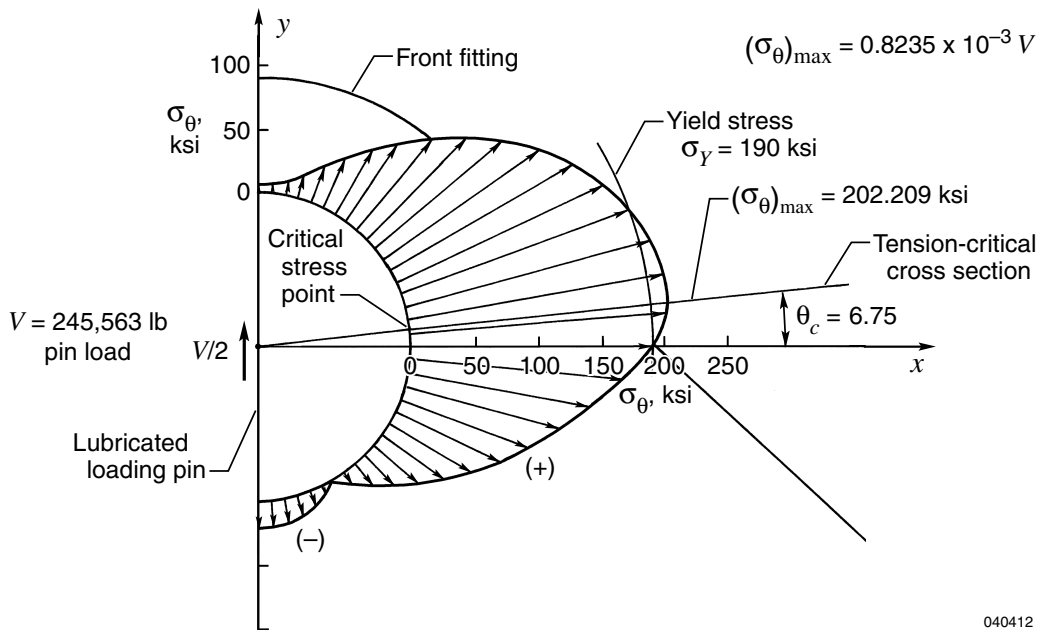


Figure 29. Distribution of tangential stress σ_{θ} along the inner pinhole boundary of the B-52H pylon front fitting.

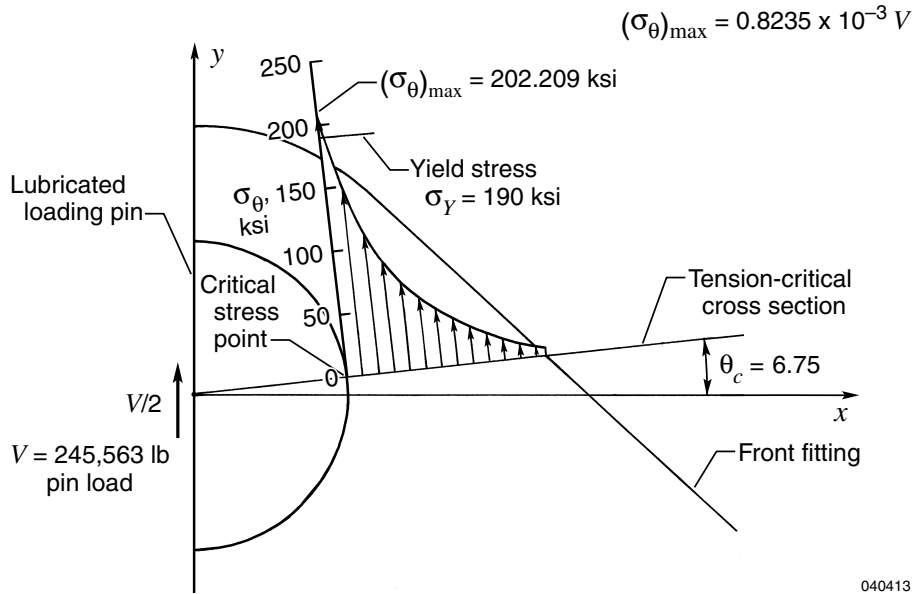


Figure 30. Distribution of tangential stress σ_{θ} along the tension-critical stress line ($\theta_c = 6.75^\circ$) of the B-52H pylon front fitting.

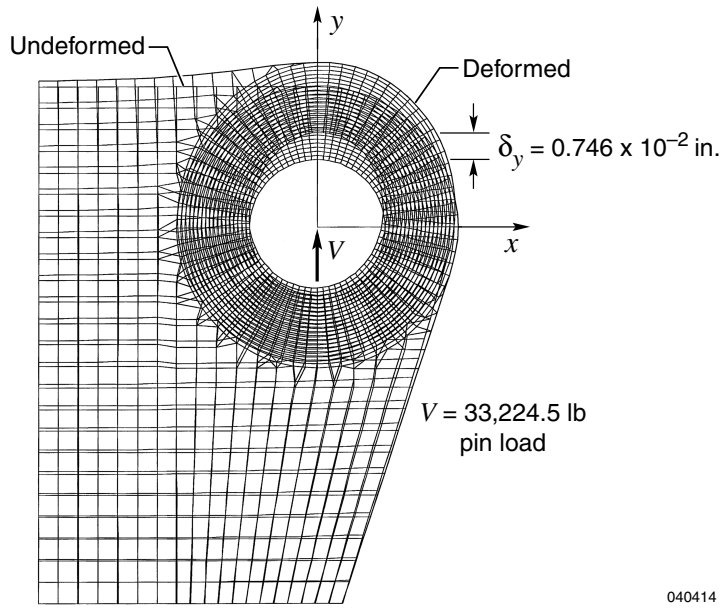


Figure 31. Deformed shape of the B-52H pylon rear fitting.

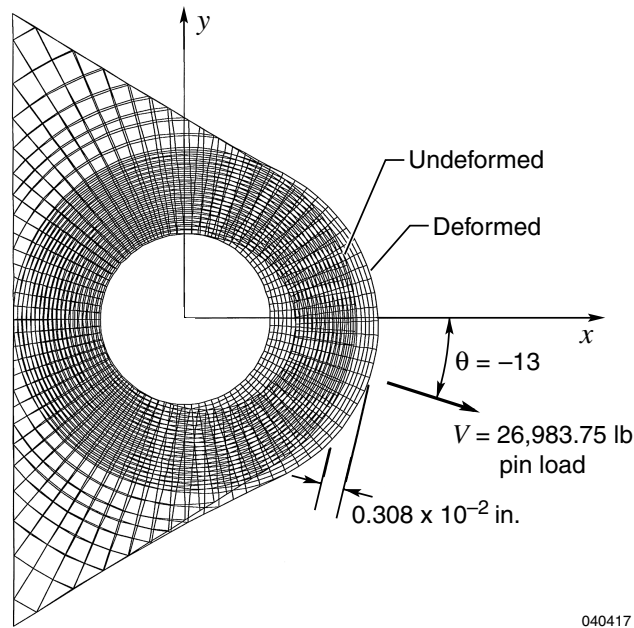


Figure 34. Deformed shape of the B-52H pylon lower sway brace.

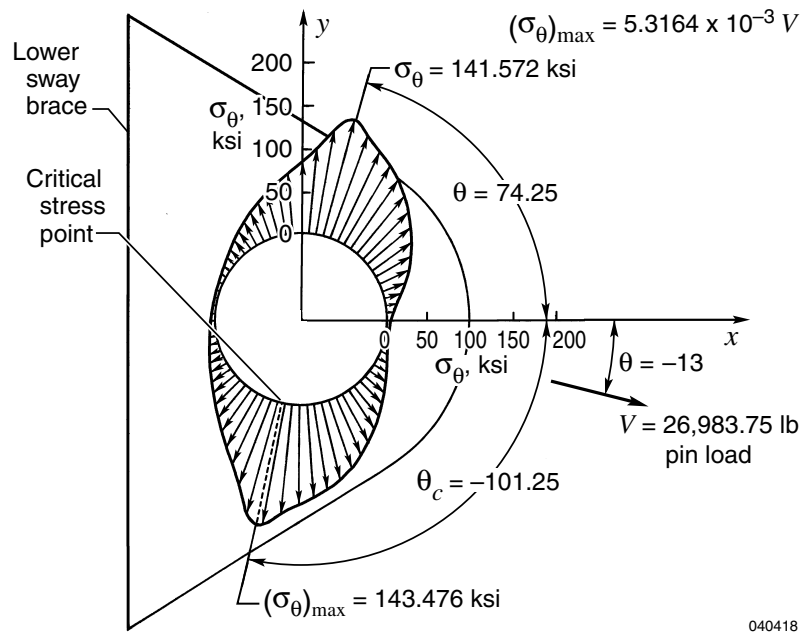


Figure 35. Distribution of tangential stress σ_{θ} along the inner pinhole boundary of the B-52H pylon lower sway brace.

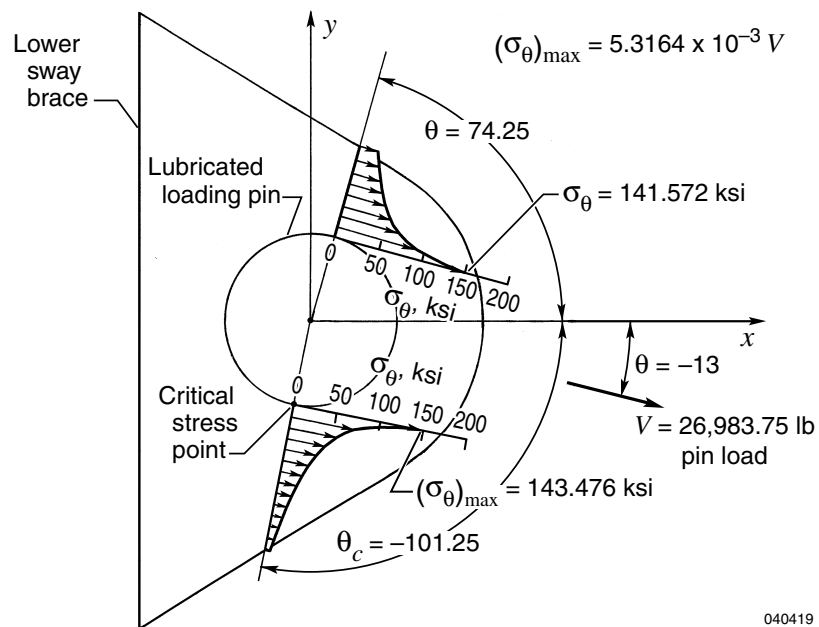


Figure 36. Distribution of tangential stress σ_θ along the critical stress line ($\theta_c = -101.25^\circ$) and radial line ($\theta = 74.25^\circ$) of the B-52H pylon lower sway brace.

APPENDIX
MATERIAL PROPERTIES

Table A-1. Material properties of failure-critical structural components of B-52B–Pegasus[®]–B-52H pylons.

Component	Material	σ_U ksi	σ_Y ksi	τ_U ksi	K_{IC} ksi $\sqrt{\text{in}}$	C $\frac{\text{in}}{\text{cycle}}(\text{ksi}\sqrt{\text{in}})^{-m}$	m	n
B-52B front hook	Inconel 718 [*]	175	145	135	125	0.922×10^{-11}	3.60	2.16
B-52B rear hooks	AMAX MP35N [†]	250	235	141	124	2.944×10^{-11}	3.24	1.69
Pegasus [®] shackles	PH13-8Mo	201	190	117	122.7	21.225×10^{-11}	2.96	1.42
Pegasus [®] hooks	AMAX MP35N [†]	250	235	141	124	2.944×10^{-11}	3.24	1.69
B-52H hooks	PH13-8Mo	201	190	117	122.7	21.225×10^{-11}	2.96	1.42
B-52H pylon front fittings	PH13-8Mo	201	190	117	122.7	21.225×10^{-11}	2.96	1.42
B-52H pylon rear fitting	PH13-8Mo	201	190	117	122.7	21.225×10^{-11}	2.96	1.42
B-52H pylon lower sway brace	PH13-8Mo	201	190	117	122.7	21.225×10^{-11}	2.96	1.42

^{*} Inconel 718 is a registered trademark of Huntington Alloy Products Division, International Nickel Company, Huntington, West Virginia.

[†] AMAX MP35N is a trademark of SPS Technologies, Inc., Jenkintown, Pennsylvania.

Table A-2. Physical properties of Inconel 718^{*}, AMAX MP35N[†] alloy and PH13-8Mo stainless steel.

Material	E , lb/in ²	G , lb/in ²	ν	ρ , lb/in ³	α , in/in- °F
Inconel 718 [*]	29.6×10^6	----	----	0.297	6.40×10^{-6}
AMAX MP35N [†]	34.05×10^6	11.74×10^6	0.390	0.322	7.10×10^{-6}
PH13-8Mo	28.30×10^6	11.00×10^6	0.280	0.279	5.80×10^{-6}

^{*} Inconel 718 is a registered trademark of Huntington Alloy Products Division, International Nickel Company, Huntington, West Virginia.

[†] AMAX MP35N is a trademark of SPS Technologies, Inc., Jenkintown, Pennsylvania.

REFERENCES

1. Ko, William L., and Lawrence S. Schuster, *Stress Analyses of B-52 Pylon Hooks*, NASA TM-84924, 1985.
2. Ko, William L., A. L. Carter, W. W. Totton, and J. M. Ficke, *Application of Fracture Mechanics and Half-Cycle Method to the Prediction of Fatigue Life of B-52 Aircraft Pylon Components*, NASA TM-88277, 1989.
3. Ko, William L., *Prediction of Service Life of Aircraft Structural Components Using the Half-Cycle Method*, NASA TM-86812, May 1987. Also in Folias, E.S., *International Journal of Fracture*, Vol. 39, pp. 45–62, Kluwer Academic Publishers, 1989.
4. Ko, William L., and Richard Monaghan, *Practical Theories for Service Life Prediction of Critical Aerospace Structural Components*, NASA TM-4354, 1992.
5. Ko, William L., Richard Monaghan, and Raymond H. Jackson, “Practical Theories for Service Life Prediction of Critical Aerospace Structural Components,” *Structural Failure, Product Liability and Technical Insurance IV— Proceedings of the 4th International Conference on Failure, Product Liability and Technical Insurance*, Vienna, Austria, July 6–9, 1992. Elsevier Science Publishers, July 1993.
6. Ko, William L., and Leslie Gong, *Thermostructural Analysis of Unconventional Wing Structures of a Hyper-X Hypersonic Flight Research Vehicle for the Mach 7 Mission*, NASA TP-2001-210398, 2001.
7. Ko, William L., *Aging Theories for Establishing Safe Life Spans of Airborne Critical Structural Components*, NASA/TP-2003-212034, 2003.
8. Whetstone, W. D., *SPAR Structural Analysis System Reference Manual, System Level 13A Vol. 1, Program Execution*, NASA CR 158970-1, 1978.
9. Ko, William L., *Stress Analysis of B-52 Pylon Hooks for Carrying the X-38 Drop Test Vehicle*, NASA TM-97-206218, 1997.

